



Growth evolution of high-quality MOCVD aluminum nitride using nitrogen as carrier gas on the sapphire substrate

Samiul Hasan^{1,a)}, Abdullah Mamun¹, Kamal Hussain¹, Mikhail Gaevski¹, Iftikhar Ahmad^{1,a)}, Asif Khan¹

Received: 9 July 2021; accepted: 10 September 2021; published online: 29 September 2021

We report the growth evolution of high-quality epitaxial aluminum nitride using nitrogen as carrier gas on the sapphire substrate using MOCVD. A series of samples were grown with thickness varying from 1 to 4 μ m utilizing a two-step process without any interlayer. SEM/AFM data showed voids up to 3 μ m thickness along the growth direction, aiding to grow thicker layers and achieve low dislocation densities. For the 4 μ m thick sample, XRD studies showed the FWHM of 289 arcsec of the rocking curve for (10 $\bar{1}$ 2) plane and total calculated dislocation density 1.1×10^9 cm⁻² using Williamson and Hall procedure. Raman's study showed the E₂ (high) phonon peak linewidth of 3.4 cm⁻¹ at around 659 cm⁻¹, showing significantly low compressive stress of 0.59 GPa for 4 μ m thick AlN. This study shows a simplified and economical method to grow high-quality AlN using N₂ as a carrier gas.

Introduction

The continued interest in epitaxially grown aluminum nitride (AlN) layers is due to their properties like ultra-wide bandgap (bandgap > 3.4 eV) and high mechanical, chemical, and thermal stability making this III-Nitride material an essential part of high temperature and high-power electronic and photonic devices [1, 2]. The high-quality AlN films have low dislocations, less strain/stress, and low surface roughness. The quality of AlN layers on sapphire substrates as a template material is the prerequisite for the low-cost production of III-nitride based devices like high-power ultraviolet light-emitting diodes (LEDs) and high electron mobility transistors (HEMTs) [3, 4]. Ideally, bulk AlN substrate can be used to fabricate better GaN/AlGaN based devices, but there is a tradeoff between device performance and cost of bulk substrates, a significant challenge for the commercialization [5-7]. The dislocations in the AlN templates can propagate into the subsequent GaN or AlGaN layers required for the device structures, creating nonradiative recombination and charge scattering centers in LEDs and HEMTs, respectively [4, 8]. In HEMTs, the higher dislocations reduce the carrier mobility in 2-dimensional electron gas (2-DEG), resulting in performance degradation [8-12]. Furthermore, a large strain field and residual stress in the AlN layer can reduce the efficiency of the UV LED structures [13]. Thus, it is desired to grow AlN layers with low dislocations, reduced strain/stress, and low surface roughness.

Several techniques have been employed to improve the quality of AlN films. These techniques include metal-organic chemical vapor deposition (MOCVD) with pulsed lateral overgrowth epitaxy [14], migration enhancement [15], modulation growth [16]. In most of these techniques, the precursors are pulsed to enhance the migration of the Al atom. The other methods to improve the quality of AlN films include high-temperature annealing under nitrogen and carbon monoxide environment [17], substrate patterning [1], use of optimized off-cut substrates [6], and annealing sputtered buffer layer [18]. It is noted that hydrogen (H₂) is used as the carrier gas in almost all the MOCVD AlN epitaxial growth processes. Kakanakova-Georgieva et al. first reported the AlN growth on SiC substrate using N₂ as carrier gas and showed, both experimentally and theoretically, that it can be beneficial [19, 20]. Miyagawa et al. reported the comparative study of N2 and H2 carrier gas-based AlN growth in the MOCVD system, but their approach using N₂ carrier gas produced inferior quality AlN samples compared

¹Department of Electrical Engineering, University of South Carolina, Columbia, SC 29208, USA

a) Address all correspondence to these authors. e-mails: shasan@email.sc.edu; ahmad@cec.sc.edu



to the samples grown with H_2 carrier gas [21]. There is no report to our knowledge, which describes the growth of *high-quality* epitaxial AlN on sapphire substrates using nitrogen (N_2) as a carrier gas by the MOCVD process, and there is not enough body of work in this regard.

This paper reports on the growth evolution of high-quality AlN on a sapphire substrate using the MOCVD process with nitrogen (N_2) as a carrier gas. We were able to grow thick, crackfree, low dislocation density, reduced residual stress, and low strain field layers of AlN on basal plane sapphire substrates. The growth involves a simple two-step process; in step one, a thin 3-dimensional (3D) buffer layer of AlN was grown on sapphire, and in the second step, thick 2-dimensional (2D) AlN layers were grown on top of the thin buffer layers, where the lateral size of these 2D layers increases with the thickness. Thus, a series of growth experiments with increasing thickness of top layers allow us to study the growth progression of AlN layers to continuous films with N_2 as a carrier gas. Table 1 provides a glancing comparison of the present work with the relevant previous results.

Results and discussion

Figure 1 shows the AFM images of the AlN buffer layers; Fig. 1a is the 0.1 μ m thick AlN buffer layer grown with N₂ as a carrier gas, and Fig. 1b is a typical 0.1 μ m AlN buffer layer grown with H₂ as a carrier gas under similar other growth conditions. The choice of low temperature (970 °C) and high V/III ratio for buffer layer growth results in low adatom mobility, which

TABLE 1: Comparison the present work with other MOCVD grown AIN.

Carrier gas	Thickness	(101 2) FWHM in arcsec	Substrate
N ₂ (this work)	3–4 μm	307–289	Sapphire
N ₂ [21]	1.0 μm	980	Sapphire
N ₂ [19]	~0.5 µm	Not mentioned	SiC
H ₂ [22]	3.0 μm	378	Sapphire

created the rough buffer layer. Here, the growth happened both in vertical and lateral directions without any preferred orientation, creating a 3D surface required to grow thick AlN. Figure 1a shows the AFM image for the buffer layer grown with N2 carrier gas and exhibits a bimodal growth. Here individual nucleation, larger, islands grew in the vertical direction (z-axis) more like pillars ('z' height around 30 nm) than the surrounding islands. This bimodal nature of the buffer layer with the N2 carrier gas is not seen with the H2 carrier gas (Fig. 1b), the reason is not clear and needs further investigation. However, we believe that the bimodal rough buffer layer is the key to the strain reduction mechanism that allows the growth of thick and crack-free AlN films with N₂ carrier gas without the requirement of interlayers. The introduction of the interlayer to grow thick AlN using H₂ carrier gas is not economical due to the longer growth time and higher cost of the hydrogen gas. In the N2 carrier grown rough layer, there are approximately 290 islands per µm² as calculated. Around 15% of the islands are with high 'z' value. On the other hand, the H₂ carrier grown rough layer has approximately 30 islands per µm² with mostly similar 'z' height. The island density values were calculated using open-source ImageJ software available on the US National Institutes of Health website, then manually verified for the smaller region. The suggested reasons for these differences are- (a) low decomposition rate of MO precursors, (b) low diffusion coefficient of reactant gases- in N₂ gas environment, and (c) low thermal conductivity of N2 carrier gas [23].

Figure 2 shows the AFM images for high-temperature AlN layers on top of 0.1 μm thick AlN buffer layers, as described before, creating the total thickness of 1 μm , 2 μm , 3 μm , and 4 μm using N_2 as a carrier gas. High growth temperature and low V/III ratio, attained by employing a higher molar flow rate of TMAl, increase the surface reaction rate, and hence the growth rate of AlN. Thus, during high-temperature growth, the Ostwald ripening occurs, and islands grow bigger, forming grains [24]. The adatoms attain enough thermal kinetic energy to mobilize

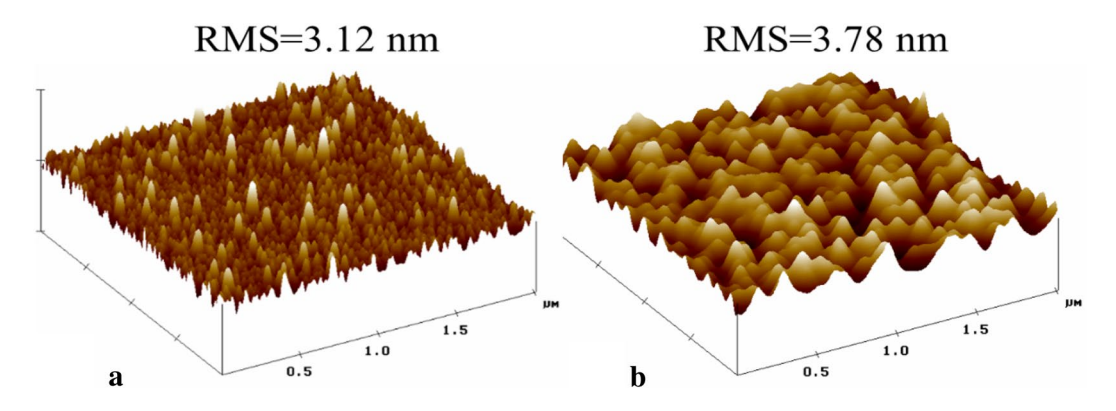


Figure 1: AFM images of AIN buffer layers grown using (a) N₂ carrier gas and (b) similar layer with H₂ carrier gas. The 'z' height scale is same for both images.



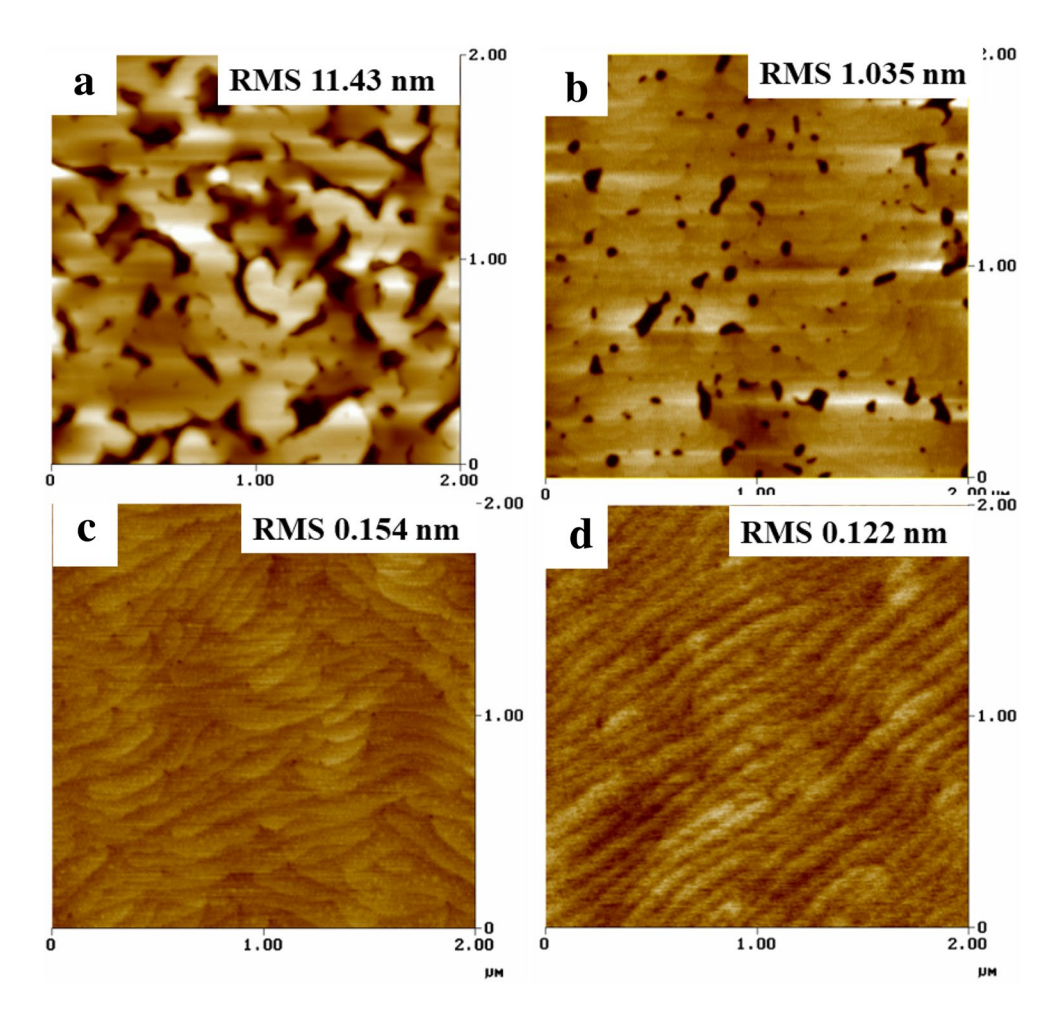


Figure 2: AFM images of AIN layers showing the surface morphology of (a) 1 µm, (b) 2 µm, (c) 3 µm, and (d) 4 µm thick samples.

and move to the surface's minimum energy positions, promoting 2D growth [25]. Thus, the 3D buffer layer supports the progression of 2D growth as the thickness of the high-temperature layer increases and desirable terrace nucleation starts to happen, which depends upon the orientation of initial domains in the buffer layer. Typically, if the samples are grown under H₂ gas, the AlN layers coalesce around 1 µm thickness. Due to the buffer layer's bimodal nature grown under the N₂ environment, as shown in Fig. 1a, the coalescence process in the lateral directions is delayed due to adatoms' restricted mobility by pillar-like structures. The growth starts from both small and large islands simultaneously, in both lateral and vertical directions. For hightemperature conditions, growth in the vertical direction is faster than in the lateral direction. Since small islands are very close to each other, they merge first. The growth from the larger islands (pillar-like structures) starts from the top of their surface. Since the larger islands are further apart from each other, their coalescence is delayed. As the growth from the larger islands continues, the material supply to smaller islands is restricted, creating voids; eventually, the larger islands become the primary origin of the final coalesced layer. At a total thickness of 1 μ m, the surface morphology had large pits between the 2D growth regions, as shown in Fig. 2a. At 2 μ m thickness, the size of the pits got reduced, as seen in Fig. 2b. The surface morphology changes until it reach an equilibrium coalescence condition [26]. The complete coalescence in AlN layers occurred around 3 μ m thickness in our growth process, as shown in Fig. 2c. This delayed coalescence helped reduce the residual stress and strain field by forming voids along the growth direction. These voids allowed us to grow thicker AlN layers without cracks shown in Fig. 2d—a 4 μ m thick AlN sample without introducing an additional intralayer or changing the growth conditions [27]. As the thickness increases, the dislocation starts to bend, and we can get low dislocation density AlN layers [28].

Figure 3 shows the cross-section SEM images of 2 μm and 3 μm samples. The cross-section SEM of the 2 μm sample shown in Fig. 3a depicts the voids and their propagation to the surface, which are exhibited as pits in the AFM image (Fig. 1b). Figure 3b shows the cross-section SEM image of a 3 μm sample; Here, we can see the void propagation up to different thicknesses, and



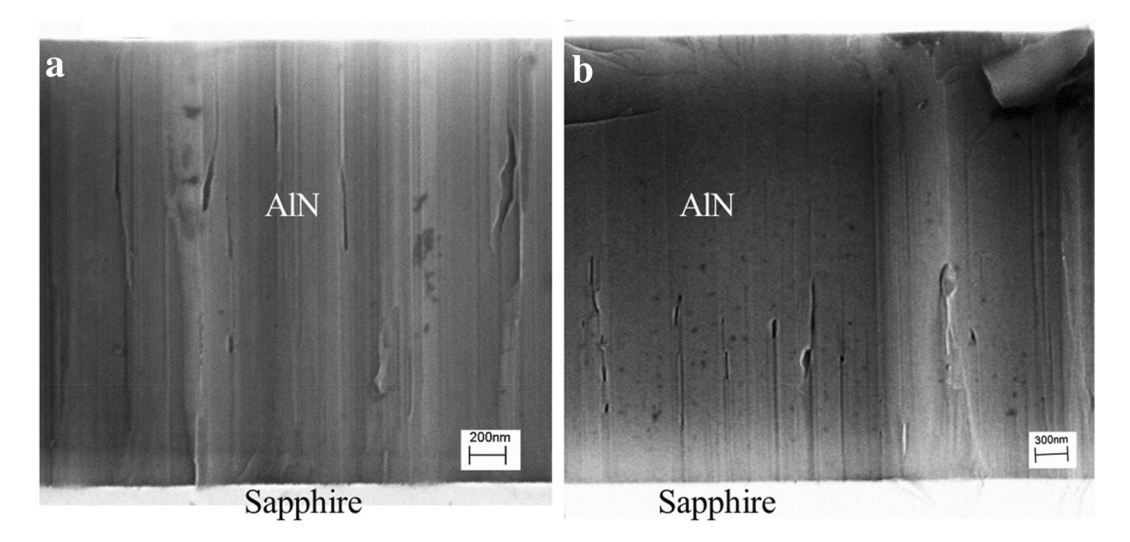


Figure 3: Cross-section SEM image showing the propagation of voids for (a) 2 μm and (b) 3 μm thick AIN samples were grown using N₂ used as carrier gas.

voids are terminated well before the surface. As seen from the AFM image Fig. 2c, the 3 μ m thick sample has a fully coalesced top surface. It has been previously demonstrated that dislocation bends, forms loops, and their numbers reduce with the thickness [29]. Thus, by growing thick AlN, reduced dislocation densities or high quality in the AlN films is achieved. Additionally, due to lattice mismatch and the residual stress, the AlN films start to crack after a specific thickness, depending on the buffer layer. The delayed coalescence of AlN using N_2 as carrier gas allows us to avoid cracking and grow thick AlN layers. The reduction in the cracks for films using H_2 as a carrier gas is achieved by introducing the interlayers [32], making the growth process complex.

Figure 4 shows the plot of fullwidth at half maxima (FWHM) of (10 $\bar{1}$ 2) ω -scan vs. thickness of the AlN layers grown using N₂ as

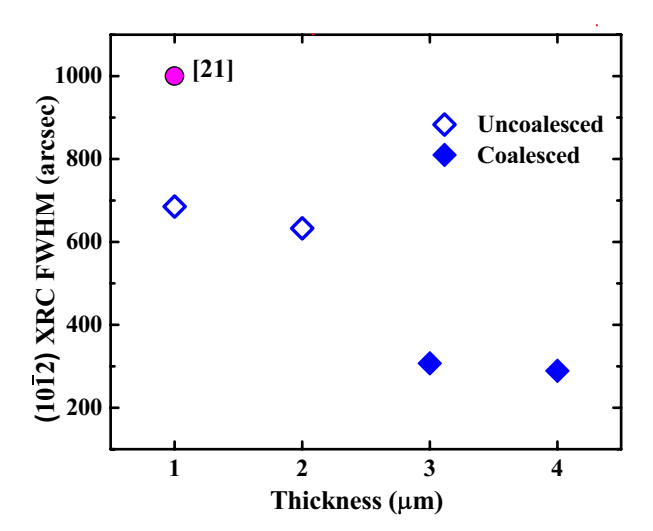


Figure 4: Thickness vs. FWHM of ω -scan for (10 $\tilde{1}$ 2) plane for AlN layers grown as described in the text.

a carrier gas. The figure also includes the only reported (10ī2) data per our knowledge for AlN produced using nitrogen as carrier gas [21]. The FWHM of the asymmetric (1012) scan of III-nitrides (AIN, GaN, and AlGaN) is directly correlated with the total dislocation densities in these materials [30]. We observed that FWHM of (10ī2) angular ω scan decreases from 685 to 289 arcsec as the thickness of AlN increases from 1 to 4 µm, indicating a reduction in dislocation densities. Note that the 1 µm and 2 µm thick AlN samples do not coalesce, as indicated by the hollow symbol, have broad FWHM. The considerable broadening of 1 μm and 2 μm uncoalesced AlN samples is mainly due to three reasons: (a) XRD samples the initial highly defective rough layer; (b) in the top layer, all the uncoalesced regions are not in the same plane; and (c) X-rays samples side-wall regions that have high dislocations as dislocations bend in the lateral directions with the increasing thickness of AlN. A significant decrease in integral linewidth for fully coalesced 3 and 4 µm samples indicates the reduction of dislocations in these layers. The uncoalesced layer acts as a secondary buffer layer to grow reduced dislocation high-quality thick AlN layers without the insertion of a low-temperature interlayer [31] or modulation of the V/III ratio [32].

The dislocation densities in AlN layers were calculated using Williamson and Hall measurements non-destructively that match well with other destructive techniques like etching and TEM measurements [33]. Williamson and Hall's measurements of the AlN layer provide information about the size and angular distribution of the mosaic blocks and means to calculate the edge and screw dislocation densities [34–36]. As we can see from Fig. 3, the uncoalesced stages of the growth had broad integral linewidth in ω -scan indicating very high dislocations due to multiple factors; thus, dislocation density was calculated only for coalesced samples. We performed symmetric and



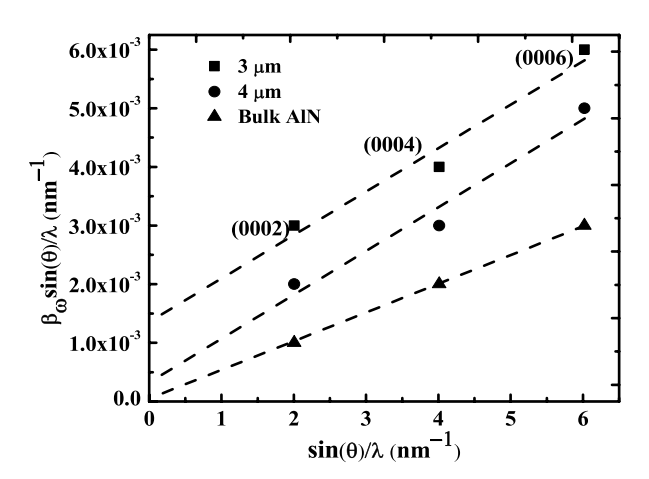


Figure 5: Representative data of Williamson and Hall measurement to calculate the dislocation density of 3 μ m, 4 μ m, and Bulk AIN samples.

asymmetric X-ray diffraction scans to determine the angular and size-dependent parameters to calculate the different types of dislocations, namely edge and screw dislocations. X-ray 2θ - ω and ω scans for symmetric planes (0002), (0004), and (0006) were used to calculate $\beta_{\omega}(\sin\theta)/\lambda$ and $\sin\theta/\lambda$ where β_{ω} is the integral linewidth of the corresponding peak in the ω -scan, θ is the angular position of theta scan, and λ is the wavelength of the X-ray used (λ = 1.5406 Å). A linear fit to the data points plotted for $\beta_{\omega}(\sin\theta)/\lambda$ vs. $\sin\theta/\lambda$ as shown in Fig. 5 was used to calculate tilt, which represents screw dislocation (N_{sc}), and the vertical intercept ($y_{0,\omega}$), which gives the lateral coherence length (L_{II}) based on equations shown below [34, 36].

$$L_{\rm II} = \frac{0.9}{2y_{0,\alpha}} \tag{1}$$

$$N_{\rm SC} = \frac{\alpha_{\omega}^2}{4.35|b_{\rm SC}|^2} \tag{2}$$

where $|b_{\rm SC}|$ is the Burger's vector ($|b_{\rm SC}|$ = 0.4982 nm, with $b_{\rm SC}$ = [0001]) for screw dislocations in AlN and directly expressed as c plane lattice constant [37, 38] and $\alpha_{\rm w}$ is the tilt angle, is the slope of the line in Fig. 5. The calculated $N_{\rm sc}$ values were in the lower 10^7 cm⁻² orders. The origin of screw dislocation density is the thermal expansion coefficient and lattice mismatch between the substrate and film [1]. It has been previously demonstrated that the creation of voids bends screw dislocations significantly, and hence thickness reduces edge dislocations [27]. We believe dislocation bending due to thickness permitted by void formation is the main reason for the low screw and edge dislocation density in the AlN sample grown with N_2 as carrier gas.

Edge dislocations (N_E) burger vector is represented as $b_E = (1/3) \ [11\overline{2}0]$ and $|b_E| = 0.311$ nm, the same as the out-of-plane lattice constant. This type of dislocation is usually generated by the azimuthal rotation of the crystallites and can be estimated from φ -scan for an asymmetric reflection and

twist angle broadening. The equation shown below is used to estimate edge dislocations (N_E): [34, 36]

$$N_E = \frac{\alpha_\varphi^2}{2.1|b_{\rm F}|L_{\rm H}} \tag{3}$$

where α_{ω} is the integral linewidth of (10ī2) φ scan.

To calculate N_E , an asymmetric (10ī2) φ scan was performed to determine the integral linewidth (α_{φ}) for each sample. Total dislocation density can be calculated as $N_T = N_E + N_{SC} + N_{\rm Mixed}$ where N_{Mixed} is mixed edge and screw dislocations. $N_{\rm Mixed}$ were ignored in N_T calculation as $N_{\rm Mixed} < N_E$ or N_{SC} [38]. The calculated N_T were the same as N_E , since N_{SC} were two orders of magnitude lower. Table 2 shows the calculated values of the screw, edge, and total dislocations densities calculated from the Williamson and Hall method along with other parameters for 3 μ m and 4 μ m thick AlN samples, including bulk the AlN for comparison. Typically the bulk AlN have total dislocations densities on the order of 10^7 cm⁻² or less, supporting the accuracy of our calculations [39].

X-ray diffraction was also used to calculate the values of in-plane lattice constant 'a' using $(10\overline{1}5)$ reciprocal space mapping, as shown in Fig. 6, based on reference [40] using Eq. (4) and to deduce the strain components (ε_{xx}) with values ranging from 0.07 to 0.14% using Eq. (5) [40],

$$a_s = \frac{2\pi}{|Q_x|} \sqrt{\frac{4(h^2 + k^2 + hk)}{3}} \tag{4}$$

$$\varepsilon_{xx} = \frac{a_s - a_e}{a_e} \times 100\% \tag{5}$$

where a_s is the in-plane lattice constant of as-grown samples, and a_e is the lattice constant for unstrained standard (a_e =0.3112 nm) [41], h=1, k=0, l=5, $|Q_x| = Q_{x(1/Å)} = (4\pi/\lambda)Q_{x(\text{rlu})}$ [42], and λ =1.5406 Å. To calculate in-plane stress, $\sigma_{xx} = (C_{11} + C_{12} - \frac{2C_{13}^2}{C_{33}})\varepsilon_{xx}$ [43, 44], the stiffness constants values are needed. There is uncertainty in stiffness constants values, depending on measurement technique or substrate type, etc. [45]. We used $C_{11} + C_{12} = 538$ GPa, $C_{13} = 113$ and $C_{33} = 370$ GPa which were used in reference [44] for MOVPE grown samples on sapphire substrates. We found compressive in-plane stress ranges from 0.35 to 0.66 GPa for 1 μ m to 4 μ m thick AlN samples.

The Raman Spectroscopy was used to corroborate the claim of high quality and low stress in MOCVD grown AlN layers characterized by X-ray diffraction. Raman spectroscopy is considered one of the most powerful tools to gauge the quality and calculate stress in thin films in a non-destructive manner [46]. Calibrated high-resolution phonon linewidth can provide information about the films' crystalline quality [47]. For the single crystal bulk AlN films, Kuball et al. reported $E_2(high)$ phonon



TABLE 2: The results of X-ray diffraction study for 3 μ m, 4 μ m, and bulk AIN

Parameters	3 µm	4 μm	Bulk AIN
Lateral coherence length, L_{\parallel} (µm)	0.21	0.35	2.55
Vertical coherence length, L_{\perp} (µm)	Layer thickness	Layer thickness	Layer thickness
Screw dislocation density, N _{SC} (cm ⁻²)	3.4×10^{7}	2.2×10^{7}	8.3×10^{6}
a_{ω} = tilt angle (arcmin)	2.18	1.74	1.03
Edge dislocation density, N_F (cm ⁻²)	2×10^{9}	1×10^{9}	6×10^7
Total dislocation density, N_T (cm ⁻²)	2×10^{9}	1×10^{9}	6.8×10^7
Off-axis (10ī2) (arcsec)	307	289	140

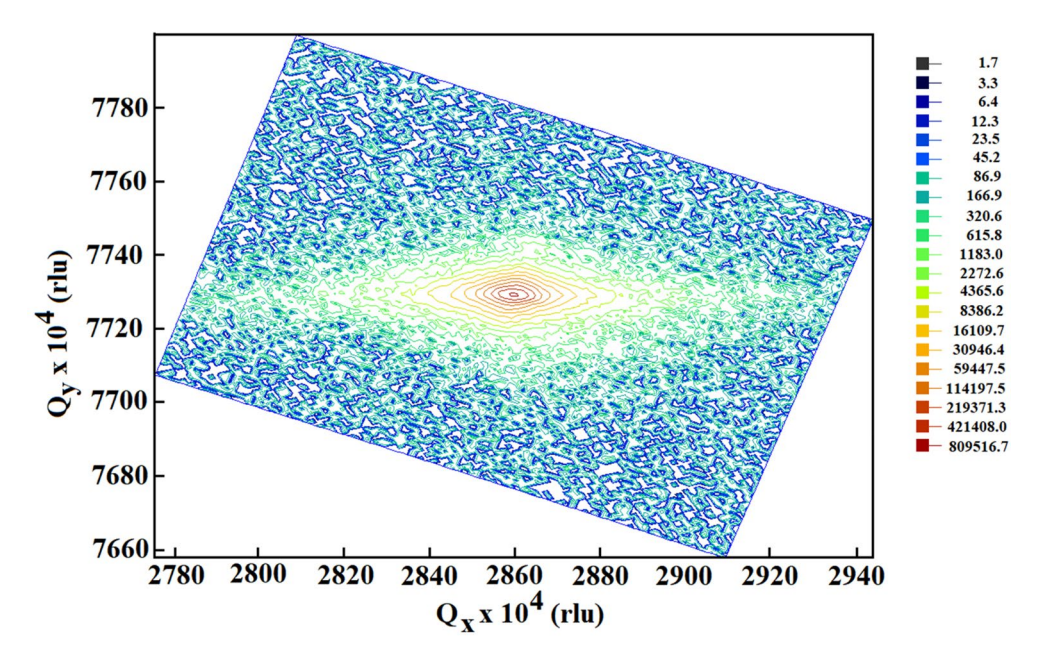


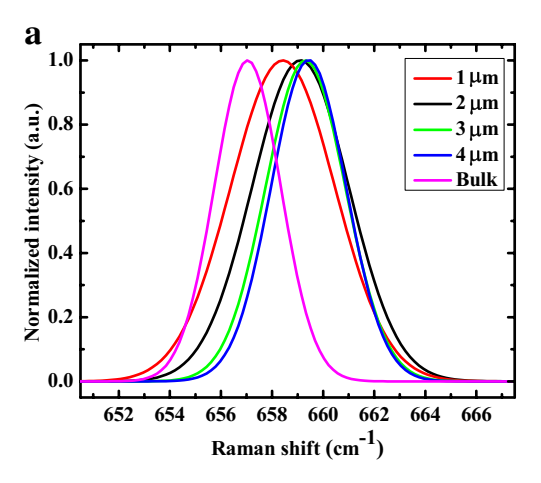
Figure 6: Reciprocal space map for (10 $\overline{1}$ 5) reflection of 3 μ m N₂ carrier grown AIN sample was used to calculate the lattice constant.

mode linewidth as 3 cm⁻¹ [48]. This value exactly matches the linewidth value found for the reference bulk AlN sample in our measurement. Under the same conditions as bulk AlN, Raman measurements of E2(high) phonon mode were performed on 1 μm to 4 μm thick grown AlN layers. The integral linewidth value ranged between 3.4 and 4.8 cm⁻¹ where the lowest value was observed for a 4 µm thick sample. The 4 µm sample also had the lowest defects shown by the Williamson and Hall measurements, confirming the high quality of the AlN film. The deviation of the E2(high) Raman peak position of MOCVD grown AlN layers from the bulk AlN (reference) was used to measure the stress in these films. Several reports have been published to establish the credibility of the biaxial stress coefficient (k)to measure stress using Raman shift in E2 (high) phonon mode [43-45]. Biaxial stress coefficient can be calculated as, $k=rac{\Delta\omega_{E2({
m high})}}{\sigma_{-\omega}}$, where $\Delta\omega_{E2({
m high})}$ is the difference between strain free frequency and MOCVD grown sample Raman shift (frequency) [43, 44]. In our calculation, we used 657.04 cm⁻¹, the bulk sample E2(high) peak position as the stress-free phonon

frequency, and calculated the stress based on $k=-4.04\pm0.3~\rm cm^{-1}/GPa$ [44, 45]. Figure 7a shows the normalized Raman spectra of E₂(high) phonon mode for the samples used in this study, including the reference bulk sample. Here, blue shift in the E₂(high) phonon from the bulk AlN indicates compressive stress in the MOCVD grown AlN layers on sapphire substrates [46].

The calculated stress value using Raman spectroscopy ranges from 0.34 ± 0.02 to 0.59 ± 0.04 GPa for 1 μm to 4 μm samples, which is in good agreement with the values calculated from the strain using XRD. The completely coalesced samples showed a high value of stress compared to uncoalesced samples. In uncoalesced samples, domains are small and randomly distributed, which allows them to relax and have low strain/stress. As soon as these domains start to merge, the film becomes strained, and the stress also increases. The compressive stress in the AlN thin film on sapphire substrate depends on lattice and thermal expansion coefficient mismatch between the epitaxial layer and substrate and generated during the cooling process of the growth. On the other hand, a tensile stress





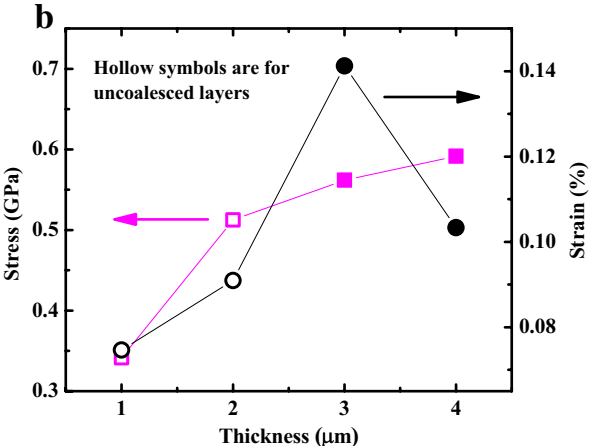


Figure 7: (a) Normalized Raman spectra of E_2 (high) phonon of MOCVD grown AIN samples on sapphire using nitrogen carrier gas, including reference bulk AIN sample. (b) The relationship between stress and strain for different thickness of AIN layers grown in N_2 environment.

is generated during the coalescence process of the sample. The resultant biaxial stress in the sample is due to the competition between the compressive and tensile stress [49, 50]. In our samples, due to the tensile stress generated during the delay in the coalescence process, the resultant overall compressive stress is low due to the unique bimodal buffer layer. Figure 7b shows the graph between stress and strain values versus film thickness. The spike in strain value for 3 μm can be due to the transition from un-coalescence to coalescence. For the 4 μm sample, strain tried to relax with more dislocation annihilation, as we can see from the decrease in dislocation density from Table 1.

Conclusions

We have demonstrated the growth progression of high-quality AlN using $\rm N_2$ as carrier gas on sapphire substrates using a two-step process. The process consists of the growth of a bimodal rough buffer layer with a high V–III ratio using pulse mode of nitrogen precursor and a low V–III ratio high Al-precursor

high-temperature continuous mode. Evidently, the bimodal rough buffer layer was the key reason which caused the delay in the AlN film's coalescence process. The uncoalesced layer allows us to grow thick AlN since the voids' formation reduces stress/strain, as seen in the combined cross-sectional SEM and X-ray/Raman studies. The transition from un-coalescence to coalescence occurs around 3 μm thickness of AlN, resulting in high-quality templates. The AlN samples grown with N_2 carrier gas are on par with AlN samples grown with the H_2 carrier gas. The research establishes a simpler, safer, and economical way to grow high-quality AlN for electronic and photonic devices.

Experimental methods

AlN layers with total thicknesses ranging from 1 to 4 µm were grown in a MOCVD reactor. The AlN epilayers were grown on 2-inch diameter c-axis sapphire substrates with 0.2° offcut towards m-plane in a custom-built vertical flow cold wall MOCVD reactor at 40 torr chamber pressure. Trimethylaluminum (TMAl) and Ammonia (NH₃) were used for aluminum (Al) and nitrogen precursors, respectively. The growth process starts with the nitridation of sapphire substrate for 2 min at 970 °C prior to the growth of 0.1 µm thick, rough (3D), AlN buffer layer at the nitridation temperature. A pulsed mode growth was used for buffer layer formation where nitrogen precursor, NH₃, with a flow of 400 standard cubic centimeters per minute (sccm), was turned on and off for 6 s. and 12 s, while TMAl material flow of 4.5 µ-mole/min was kept on for the whole growth sequence. This step is depicted in Fig. 8a, and the resulting 3D AlN layer is shown in Fig. 8b schematically. The V/III ratio in this layer was kept around 4000 (the exact ratio is 3965) and was calculated as the average of NH₂ on and off states. After the buffer layer, in the second step, the temperature was ramped up to 1180 °C to grow the thick AlN top layer using the same precursors with continuous NH3 flow with V/III ratio decreased to ~ 1000 (the exact ratio is 1114) by increasing the TMAl flow to 16 μ-mole/min. The second step in the growth is shown in Fig. 8c, and the resulting AlN layer is illustrated in Fig. 8d schematically for four micrometer thick sample. A series of samples with the same buffer layer and high-temperature top AlN layers with total thicknesses from 1 to 4 µm were grown. For all the samples, the growth rate for the high-temperature layer was around 1 µm/h. The growth in succession allows us to observe the growth evolution of the AlN layer to an entire 2D top surface.

The grown AlN films were characterized for their surface morphology, dislocation densities, strain field, and residual stress. The surface morphology of grown AlN was observed with Digital Nanoscope 3100, atomic force microscopy (AFM). Philips X'pert MRD triple-axis diffractometer with Cu-K α 1 X-ray source was used to calculate the strain and dislocation densities. We used a commercial



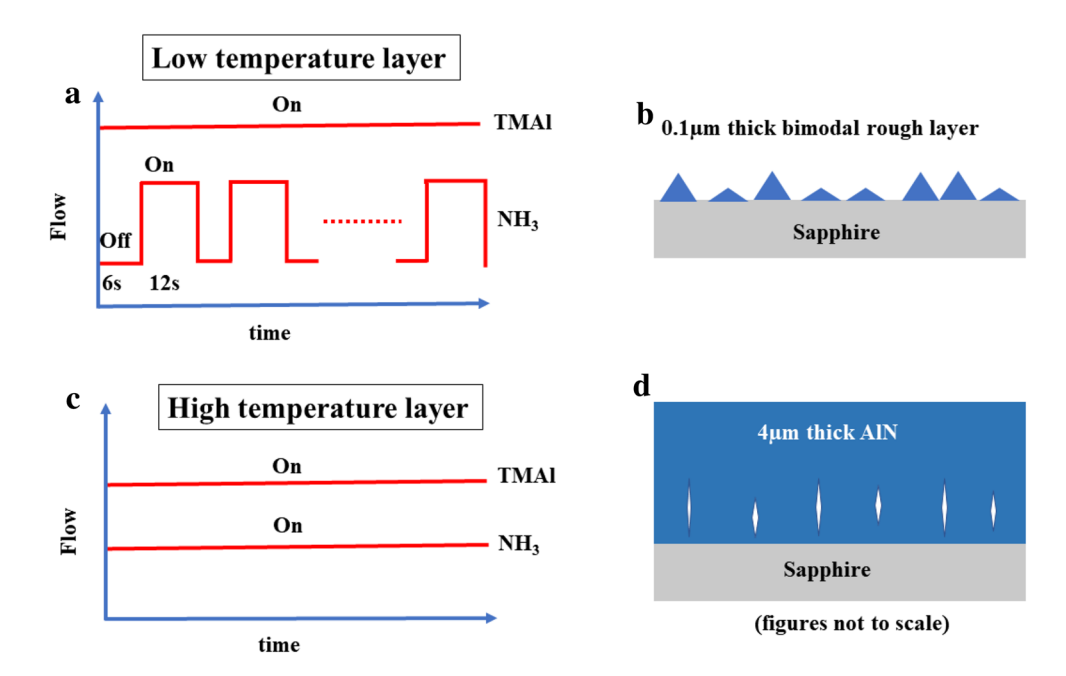


Figure 8: Schematic of the process for AlN growth with the N_2 carrier gas; (a) precursors flow for low-temperature pulsed growth, (b) result in the rough buffer layer, (c) precursors flow for high-temperature continuous growth, (d) resulting 4 μ m thick AlN layer.

XRD system with a Ge(220) fourfold Bartels-type monochromator and a Ge(220) threefold analyzer to perform 2θ – ω scans and ω rocking curves—a configuration described by Fewster et al. [51]. For optimization, we used 0.2 mm, and 0.3 mm for the incident and receiving slit, respectively; for actual measurement, these values are 0.05 mm and 0.05 and preserved for all the measurements. A scanning electron microscope (SEM) Zeiss Supra 25 FE-SEM was used to study the AlN samples' cross-sections along the growth direction. Residual stress in the samples was measured by Raman spectroscopy using Horiba Raman Spectroscope with a 638 nm red excitation laser with 25% power. 2400 g/mm grating was used with 100 μ m hole size and 50 μ m slit size in backscattered mode with a spectral resolution of 0.5 cm⁻¹.

Acknowledgments

This work was supported by the National Science Foundation (NSF) Award No. 2124624 managed by Dr. Dominique M. Dagenais and SCEEE research initiation grant for 2021–2022.

Data availability

The data generated during and/or analyzed during the current study are available from the corresponding authors on reasonable request.

Declarations

Conflict of interest The authors declare that they have no conflict of interest.

References

- H. Long, J. Dai, Y. Zhang, S. Wang, B. Tan, S. Zhang, L. Xu, M. Shan, Z.C. Feng, H.C. Kuo, C. Chen, High quality 10.6 μm AlN grown on pyramidal patterned sapphire substrate by MOCVD. Appl. Phys. Lett. 114(4), 1 (2019)
- Y. Taniyasu, M. Kasu, T. Makimoto, An aluminium nitride lightemitting diode with a wavelength of 210 nanometres. Nature 441(7091), 325 (2006)
- J.Y. Tsao, S. Chowdhury, M.A. Hollis, D. Jena, N.M. Johnson, K.A. Jones, R.J. Kaplar, S. Rajan, C.G. Van de Walle, E. Bellotti, C.L. Chua, R. Collazo, M.E. Coltrin, J.A. Cooper, K.R. Evans, S. Graham, T.A. Grotjohn, E.R. Heller, M. Higashiwaki, M.S. Islam, P.W. Juodawlkis, M.A. Khan, A.D. Koehler, J.H. Leach, U.K. Mishra, R.J. Nemanich, R.C.N. Pilawa-Podgurski, J.B. Shealy, Z. Sitar, M.J. Tadjer, A.F. Witulski, M. Wraback, J.A. Simmons, Ultrawide-bandgap semiconductors: research opportunities and challenges. Adv. Electron. Mater. 4(1), 1600501 (2018)
- H. Hirayama, S. Fujikawa, J. Norimatsu, T. Takano, K. Tsubaki, N. Kamata, Fabrication of a low threading dislocation density ELO-AlN template for application to deep-UV LEDs. Phys. Status Solidi Curr. Top. Solid State Phys. 6(SUPPL 2), 2 (2009)
- C. Liu, Y. Zhang et al., Investigation of AlGaN/GaN heterostructures grown on sputtered AlN templates with different nucleation layers. Materials 12(24), 4050 (2019)
- A. Knauer, A. Mogilatenko, S. Hagedorn, J. Enslin, T. Wernicke, M. Kneissl, M. Weyers, Correlation of sapphire off-cut and reduction of defect density in MOVPE grown AlN. Phys. Status Solidi Basic Res. 253(5), 809 (2016)



- X. Sun, D. Li, Y. Chen, H. Song, H. Jiang, Z. Li, G. Miao, Z. Zhang, In situ observation of two-step growth of AlN on sapphire using high-temperature metal-organic chemical vapour deposition. CrystEngComm 15(31), 6066 (2013)
- D. Jena, A.C. Gossard, U.K. Mishra, Dislocation scattering in a two-dimensional electron gas. Appl. Phys. Lett. 76(13), 1707 (2000)
- F.A. Marino, N. Faralli, T. Palacios, D.K. Ferry, S.M. Goodnick, M. Saraniti, Effects of threading dislocations on AlGaN/GaN high-electron mobility transistors. IEEE Trans. Electron Devices 57(1), 353 (2010)
- Y.J. Cho, Y. Ren, H.G. Xing, D. Jena, High-mobility two-dimensional electron gases at AlGaN/GaN heterostructures grown on GaN bulk wafers and GaN template substrates. Appl. Phys. Express 12(12), 8 (2019)
- Y.-Y. Wong, E.Y. Chang, T.-H. Yang, J.-R. Chang, J.-T. Ku, M.K. Hudait, W.-C. Chou, M. Chen, K.-L. Lin, The roles of threading dislocations on electrical properties of AlGaN/GaN heterostructure grown by MBE. J. Electrochem. Soc. 157(7), H746 (2010)
- S.W. Kaun, P.G. Burke, M. Hoi Wong, E.C.H. Kyle, U.K. Mishra, J.S. Speck, Effect of dislocations on electron mobility in AlGaN/ GaN and AlGaN/AlN/GaN heterostructures. Appl. Phys. Lett. 101(26), 262102 (2012)
- S. Yang, R. Miyagawa, H. Miyake, K. Hiramatsu, H. Harima, Raman scattering spectroscopy of residual stresses in epitaxial AlN films. Appl. Phys. Express 4(3), 10 (2011)
- Z. Chen, R.S. Qhalid Fareed, M. Gaevski, V. Adivarahan, J.W. Yang, A. Khan, J. Mei, F.A. Ponce, Pulsed lateral epitaxial overgrowth of aluminum nitride on sapphire substrates. Appl. Phys. Lett. 89(8), 081905 (2006)
- R. Jain, W. Sun, J. Yang, M. Shatalov, X. Hu, A. Sattu, A. Lunev, J. Deng, I. Shturm, Y. Bilenko, R. Gaska, M.S. Shur, Migration enhanced lateral epitaxial overgrowth of AlN and AlGaN for high reliability deep ultraviolet light emitting diodes. Appl. Phys. Lett. 93(5), 10 (2008)
- Z. Chen, S. Newman, D. Brown, R. Chung, S. Keller, U.K. Mishra, S.P. Denbaars, S. Nakamura, High quality AlN grown on SiC by metal organic chemical vapor deposition. Appl. Phys. Lett. 93(19), 91 (2008)
- H. Miyake, G. Nishio, S. Suzuki, K. Hiramatsu, H. Fukuyama, J. Kaur, N. Kuwano, Annealing of an AlN buffer layer in N₂-CO for growth of a high-quality AlN film on sapphire. Appl. Phys. Express 9(2), 025501 (2016)
- C. He, W. Zhao, H. Wu, S. Zhang, K. Zhang, L. He, N. Liu, Z. Chen, B. Shen, High-quality AlN film grown on sputtered AlN/ sapphire via growth-mode modification. Cryst. Growth Des. 18(11), 6816 (2018)
- A. Kakanakova-Georgieva, A. Kasic, C. Hallin, B. Monemar, E. Janzén, Performance of III-nitride epitaxy in a low V-to-III gas-flow ratio range under nitrogen ambient in a hot-wall MOCVD system. Phys. Status Solidi C 2(3), 960 (2005)

- A. Kakanakova-Georgieva, G.K. Gueorguiev, S. Stafström, L. Hultman, E. Janzén, AlGaInN metal-organic-chemical-vapordeposition gas-phase chemistry in hydrogen and nitrogen diluents: first-principles calculations. Chem. Phys. Lett. 431(4–6), 346 (2006)
- R. Miyagawa, S. Yang, H. Miyake, K. Hiramatsu, Effects of carrier gas ratio and growth temperature on MOVPE growth of AlN. Phys. Status Solidi Curr. Top. Solid State Phys. 9(3–4), 499 (2012)
- C.P. Huang, C.H. Wang, C.P. Liu, K.Y. Lai, High-quality AlN grown with a single substrate temperature below 1200 C. Sci. Rep. 7, 1–6 (2017)
- X. Su, T. Ye, S. Wang, Y. Shi, L. Fan, L. Liu, G. Zhang, X. Shi, M. Wei, H. Zhou, H. Jiao, Surface morphology of GaN nucleation layer grown by MOCVD with different carrier gas. AIP Adv. 8(7), 1 (2018)
- 24. C. Ratsch, J.A. Venables, Nucleation theory and the early stages of thin film growth. J. Vac. Sci. Technol. A 21(5), 96 (2003)
- D. Magnfält, Fundamental processes in thin film growth: the origin of compressive stress and the dynamics of the early growth stages, PhD Dessertation, Linköping University (2014)
- C.V. Thompson, Structure evolution during processing of polycrystalline films. Annu. Rev. Mater. Sci. 30, 159 (2000)
- H. Sun, F. Wu, T.M. Al Tahtamouni, N. Alfaraj, K.H. Li, T. Detchprohm, R.D. Dupuis, X. Li, Structural properties, crystal quality and growth modes of MOCVD-grown AlN with TMAl pretreatment of sapphire substrate. J. Phys. D 50(39), 395101 (2017)
- K. Balakrishnan, K. Iida, A. Bandoh, M. Iwaya, S. Kamiyama, H. Amano, I. Akasaki, Void assisted dislocation reduction in AlN and AlGaN by high temperature MOVPE. Phys. Status Solidi Curr. Top. Solid State Phys. 4(7), 2272 (2007)
- C. He, W. Zhao, H. Wu, N. Liu, S. Zhang, J. Li, C. Jia, K. Zhang, L. He, Z. Chen, B. Shen, Fast growth of crack-free thick AlN film on sputtered AlN/sapphire by introducing high-density nano-voids. J. Phys. D 53(40), 405303 (2020)
- S.C. Jain, M. Willander, J. Narayan, R. Van, Overstraeten, III– nitrides: growth, characterization, and properties. J. Appl. Phys. 87(3), 965–1006 (2000)
- Y. Guo, Y. Fang, J. Yin, Z. Zhang, B. Wang, J. Li, W. Lu, Z. Feng, Improved structural quality of AlN grown on sapphire by 3D/2D alternation growth. J. Cryst. Growth 464, 119–122 (2017)
- B. Tan, J. Hu, J. Zhang, Y. Zhang, H. Long, J. Chen, S. Du, J. Dai,
 C. Chen, J. Xu, F. Liu, X. Li, AlN gradient interlayer design for
 the growth of high-quality AlN epitaxial film on sputtered AlN/
 sapphire substrate. CrystEngComm 20(41), 6557 (2018)
- V. Ivantsov, A. Volkova, A comparative study of dislocations in HVPE GaN layers by high-resolution X-ray diffraction and selective wet etching. ISRN Condens. Matter. Phys. 2012, 1 (2012)
- T. Metzger, R. Höpler, E. Born, O. Ambacher, M. Stutzmann, R. Stömmer, M. Schuster, H. Göbel, S. Christiansen, Defect structure of epitaxial GaN films determined by transmission electron



- microscopy and triple-axis X-ray diffractometry. Philos. Mag. A 77(4), 1013 (1998)
- H. Fitouri, M.M. Habchi, A. Rebey, H. Fitouri, M.M. Habchi, A. Rebey, High-resolution X- ray diffraction of III–V semiconductor films high-resolution thin diffraction of III–V semiconductor thin films. X-Ray Scatt. (2017). https://doi.org/10.5772/65404
- H.M. Wang, J.P. Zhang, C.Q. Chen, Q. Fareed, J.W. Yang, M.A. Khan, AlN/AlGaN superlattices as dislocation filter for lowthreading-dislocation thick AlGaN layers on sapphire. Appl. Phys. Lett. 81(4), 604 (2002)
- P. Bhattacharya, L.Y. Pang, Semiconductor optoelectronic devices. Phys. Today 47(12), 64 (1994)
- I. Ferguson, Study of residual strain in large area AlGaN growth and characterization support. DARPA Technical Report. Georgia Institute of Technology (2004)
- I. Satoh, S. Arakawa, K. Tanizaki, M. Miyanaga, T. Sakurada,
 Y. Yamamoto, H. Nakahata, Development of aluminum nitride single-crystal substrates. SEI Tech. Rev. 79(71), 78 (2010)
- Y. Feng, V. Saravade, T.F. Chung, Y. Dong, H. Zhou, B. Kucukgok, I.T. Ferguson, N. Lu, Strain-stress study of AlxGa1-xN/AlN heterostructures on c-plane sapphire and related optical properties. Sci. Rep. 9(1), 1 (2019)
- W.M. Yim, E.J. Stofko, P.J. Zanzucchi, J.I. Pankove, M. Ettenberg,
 S.L. Gilbert, Epitaxially grown AlN and its optical band gap. J.
 Appl. Phys. 44(1), 292 (1973)
- 42. M.A. Moram, M.E. Vickers, X-ray diffraction of III-nitrides. Rep. Prog. Phys. **72**(3), 036502 (2009)
- 43. M.X. Wang, F.J. Xu, N. Xie, Y.H. Sun, B.Y. Liu, W.K. Ge, X.N. Kang, Z.X. Qin, X.L. Yang, X.Q. Wang, B. Shen, High-temperature annealing induced evolution of strain in AlN epitaxial films

- grown on sapphire substrates. Appl. Phys. Lett. **114**(11), 112105 (2019)
- S. Yang, R. Miyagawa, H. Miyake, K. Hiramatsu, H. Harima, Raman scattering spectroscopy of residual stresses in epitaxial AlN films. Appl. Phys. Express 4(3), 031001 (2011)
- T. Prokofyeva, M. Seon, J. Vanbuskirk, M. Holtz, S.A. Nikishin, N.N. Faleev, H. Temkin, S. Zollner, Vibrational properties of AlN grown on (111)-oriented silicon. Phys. Rev. B (2001). https://doi. org/10.1103/PhysRevB.63.125313
- M. Kuball, Raman spectroscopy of GaN, AlGaN and AlN for process and growth monitoring/control. Surf. Interface Anal. 31(10), 987 (2001)
- M. Kuball, J.M. Hayes, Y. Shi, J.H. Edgar, A.D. Prins, N.W.A. Van Uden, D.J. Dunstan, Raman scattering studies on single-crystalline bulk AlN: temperature and pressure dependence of the AlN phonon modes. J. Cryst. Growth 231(3), 391 (2001)
- M. Kuball, J.M. Hayes, A.D. Prins, N.W.A. Van Uden, D.J. Dunstan, Y. Shi, J.H. Edgar, Raman scattering studies on single-crystalline bulk AIN under high pressures. Appl. Phys. Lett. 78(6), 724 (2001)
- H. Harima, Properties of GaN and related compounds studied by means of Raman scattering. J. Phys. Condens. Matter. (2002). https://doi.org/10.1088/0953-8984/14/38/201
- X. Rong, X. Wang, G. Chen, J. Pan, P. Wang, H. Liu, F. Xu, P. Tan, B. Shen, Residual stress in AlN films grown on sapphire substrates by molecular beam epitaxy. Superlattices Microstruct. 93, 27 (2016)
- P.F. Fewster, N.L. Andrew, Absolute lattice-parameter measurement. J. Appl. Crystallogr. 28(4), 451 (1995)